

Interaction between fluids and Helfrich layers

Michele Castellana^{1,2}

¹*Institut Curie, PSL Research University, Paris, France*

²*CNRS UMR168, 11 rue Pierre et Marie Curie, 75005, Paris, France*

(Dated: January 7, 2026)

1. [1] study the steady state with arc-length gauge
2. In the dynamics, arc-length gauge does not work
3. We show how to use a generalized arc-length gauge and how to correctly incorporate it into the dynamics to obtain a proper dynamics, Fig. 6.
4. In this dynamics
 - we implement the Crank-Nicolson method to the equations written in the reference configuration, and prove it to be numerically stable
 - we show that the derivative of mesh motion $\dot{\mathbf{u}}_D$ can be obtained exactly from an auxiliary PDE without recurring to error-prone time discretization.
5. We couple the membrane dynamics to a bulk fluid. The membrane is a complex elastic body -i. We proceed by steps:
 - (a) Bulk fluid + rigid body Fig. 2
 - (b) Elastic body with stable elastic model (stable under compression)
 - (c) Bulk fluid + elastic body with stable elastic model, Fig. 5
 - (d) Bulk fluid + membrane, Fig. 7
 - Bulk fluid and membrane both described with Crank-Nicolson method -i. we prove that the resulting dynamics is numerically stable. Say that you found a way to replace $t \rightarrow t_n$ that is stable and that you could have used other ways which are also correct to within $\mathcal{O}(\Delta t)$.
 - It allows for overhangs
 - It is the first study that describes a bulk fluid coupled to a Helfrich membrane with ALE

- It allows for turbulent behavior for both the bulk fluid and the membrane tangential flow

Perspectives:

1. Study nucleoid compaction in E. Coli with ALE

I. FLUID AND RIGID BODY

In this Section, we will discuss the interaction between a **bulk fluid** (**F**) and the simplest structure—a **rigid body** (**R**) which is only allowed to turn about one point.

In all the systems that we will consider, we will introduce the **reference** (**r**) and **current** (**c**) configuration [2–4], see Fig. 1. All quantities relative to the **r** and **c** configuration will be denoted by the superscript **r** and **c**, respectively. In the **r** configuration, the region occupied by the bulk fluid is described by Cartesian coordinates \mathbf{x}_r . The axis of the ellipse, e.g., the rigid body, lies parallel to the x_c^1 axis. In the **c** configuration, the region occupied by the bulk fluid is described by Cartesian coordinates \mathbf{x}_c . The axis of the ellipse, e.g., the rigid body, forms an angle θ (red arc) with respect to the x_c^1 axis.

The **r** configuration, is related to the **c** one as follows [2], see Fig. 1. At time t , the point \mathbf{x}_c corresponds to a point \mathbf{x}_r in the reference configuration through the deformation field [5]

$$\mathbf{u}_D^t(\mathbf{x}_r) \equiv \mathbf{x}_c - \mathbf{x}_r. \quad (1)$$

and the deformation-gradient tensor

$$F_{\alpha\beta}(\mathbf{u}) \equiv \delta_{\alpha\beta} + \frac{\partial u^\alpha}{\partial x_r^\beta}, \quad (2)$$

read [6]

where we set

$$\partial_{\alpha}^r \equiv \frac{\partial}{\partial x_r^{\alpha}}, \quad (3)$$

$$\partial_{\alpha}^c \equiv \frac{\partial}{\partial x_c^{\alpha}}. \quad (4)$$

Here, we will denote the mapping between \mathbf{x}_c and \mathbf{x}_r in Eq. (1) with the fields

$$\mathbf{x}_c = \varphi^t(\mathbf{x}_r), \quad (5)$$

$$\mathbf{x}_r = \psi^t(\mathbf{x}_c). \quad (6)$$

We denote the \mathbf{F} velocity and surface tension by $v_c(\mathbf{x}_c)$ and $\sigma_c(\mathbf{x}_c)$, respectively, where the superscript c specifies that these fields depend on the coordinate \mathbf{x}_c in the c configuration.

The solution of the interaction dynamics between \mathbf{F} and \mathbf{R} is involved because of the presence of the moving boundary $\partial\Omega_c^c$, cf. Fig. 1. Following the arbitrary Lagrangian-Eulerian (ALE) procedure, we will bridge between the Lagrangian and the Eulerian description used to describe, respectively, \mathbf{R} and \mathbf{F} [2]. To achieve this, in what follows we will write the equations of motion for \mathbf{R} and \mathbf{F} , which are naturally formulated the c configuration first, and then rewrite them in the r configuration.

A. Rigid body motion

In this Section, we will work out the equations of motion for \mathbf{R} .

1. Equation of motion in the *current*-configuration coordinates

The dynamics of \mathbf{R} is given by the equations of motion for a rigid body which, in c coordinates,

Equation (7) relates the angular acceleration of \mathbf{R} to the torque of external forces. In what follows, Greek indices α, β, \dots will be used to denote vectors and tensors in two-dimensional Euclidean space—their

position as upper or lower indices is thus immaterial [3, 7]. The moment of inertia of \mathbf{R} is denoted by I . The right-hand side (RHS) of Eq. (7) contains the line integral along the boundary of \mathbf{R} , of the torque of the local force exerted by \mathbf{F} on \mathbf{R} with respect to the left focal point \mathbf{f} of \mathbf{R} [5]. This force is expressed in terms of the \mathbf{F} stress tensor [5]

$$\varsigma^c_{\alpha\beta} \equiv \sigma_c \delta_{\alpha\beta} + \eta_F \left(\frac{\partial v_c^\alpha}{\partial x_c^\beta} + \frac{\partial v_c^\beta}{\partial x_c^\alpha} \right), \quad (9)$$

where $\epsilon_{\alpha\beta\gamma}$ is the three-dimensional Levi-Civita symbol, and η_F the two-dimensional viscosity of \mathbf{F} . Finally, dl_c is the line element of $\partial\Omega_c^c$ in the c configuration, and $\hat{\mathbf{n}}^c$ the unit boundary normal to $\partial\Omega_c^c$ pointing outside Ω^c .

2. Equation of motion in the *reference*-configuration coordinates

$$I \frac{d\omega}{dt} = \int_{\partial\Omega_c^r} ds \epsilon_{\alpha\beta} [\varphi^{\alpha,t}(\xi(s)) - f^\alpha] \varsigma^r_{\beta\gamma}(\xi(s)) \epsilon_{\gamma\lambda} F_{\lambda\mu}(\mathbf{u}_D^t(\xi(s))) \frac{d\xi^\mu(s)}{ds} \quad (10)$$

In Eq. (10), the integral in the RHS is over the

curvilinear boundary $\partial\Omega_c^r$, which is parametrized

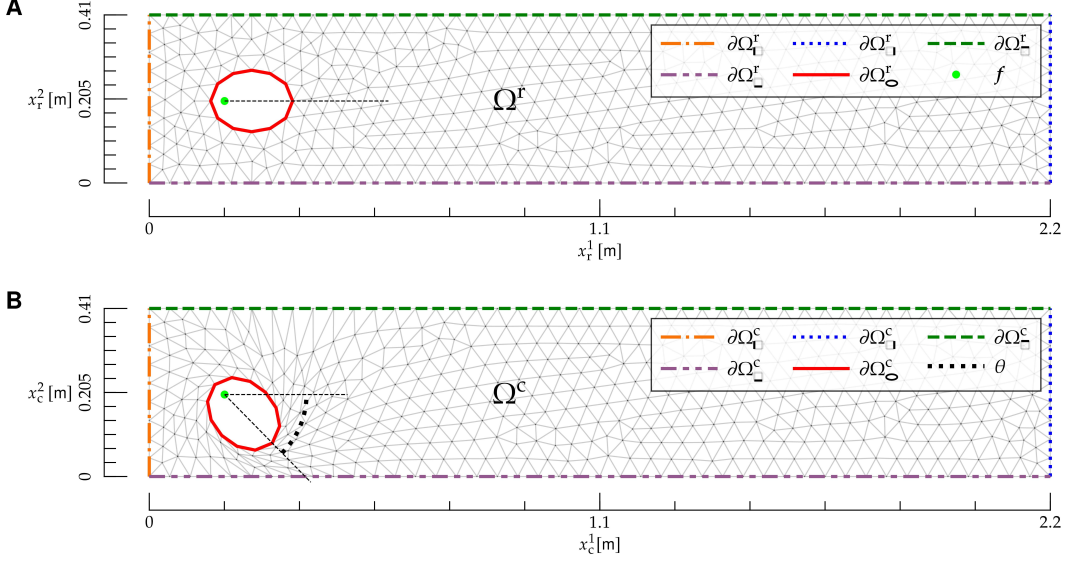


FIG. 1: Reference and current configuration for the interaction between a bulk fluid and a rigid body. **A)** Reference configuration. The region Ω^r is given by the rectangle $0 \leq x_r^1 \leq L$, $0 \leq x_r^2 \leq h$ with the elliptical hole, and is delimited by the mesh (gray lines). Boundaries in the reference configuration are denoted by $\partial\Omega_{\square}^r$, $\partial\Omega_{\square}^r$, $\partial\Omega_{\square}^r$, $\partial\Omega_{\square}^r$ and $\partial\Omega_{\square}^r$ (colored dashed lines). The ellipse focal point f (light green dot) is also shown. **B)** Current configuration. The region Ω^c is delimited by the mesh (gray lines). Boundaries in the current configuration are denoted by $\partial\Omega_{\square}^c$, $\partial\Omega_{\square}^c$, $\partial\Omega_{\square}^c$, $\partial\Omega_{\square}^c$ and $\partial\Omega_{\square}^c$ (colored dashed lines), and the rotational angle θ of the rigid body is shown as an arc (black dotted line). The Cartesian coordinates \mathbf{x}_c are also shown.

as $\mathbf{x}_r = \xi(s)$, where s is the curvilinear coordinate. Also, $\epsilon_{\alpha\beta}$ is the two-dimensional Levi-Civita symbol [7], and ς^r denotes the stress tensor in the r configuration:

$$\begin{aligned} \varsigma^{rt}_{\alpha\beta}(\mathbf{x}_r) &\equiv \varsigma^c_{\alpha\beta}(\varphi^t(\mathbf{x}_r)) \\ &= \sigma_r(\mathbf{x}_r, t)\delta_{\alpha\beta} + \eta_F \left[G_{\gamma\beta}(\mathbf{u}_D^t(\mathbf{x}_r)) \frac{\partial v_c^\alpha}{\partial x_r^\gamma} + \right. \\ &\quad \left. G_{\gamma\alpha}(\mathbf{u}_D^t(\mathbf{x}_r)) \frac{\partial v_c^\beta}{\partial x_r^\gamma} \right], \end{aligned} \quad (11)$$

where

$$G_{\alpha\beta}(\mathbf{u}) \equiv [F(\mathbf{u})]_{\alpha\beta}^{-1}. \quad (12)$$

B. Fluid motion

In this Section, we will work out the equations of motion for \mathbf{F} .

1. Equations of motion in the current-configuration coordinates

The equations of motion, expressed in terms of the c fields v_c and σ_c , are

$$\rho_F \left(\partial_t v_c^\alpha + v_c^\beta \frac{\partial v_c^\alpha}{\partial x_c^\beta} \right) = \frac{\partial \sigma_c}{\partial x_c^\alpha} + \eta_F \frac{\partial}{\partial x_c^\beta} \frac{\partial v_c^\alpha}{\partial x_c^\beta}, \quad (13)$$

$$\frac{\partial v_c^\alpha}{\partial x_c^\alpha} = 0, \quad (14)$$

and they hold for $x_c \in \Omega^c$. Equations (13) and (14) are the Navier-Stokes (NS) and continuity equation, respectively, in a flat, two-dimensional geometry [5]—an example of the NS equations on curved geometry will be presented in X. There, ρ_F is the two-dimensional F density.

The boundary conditions (BCs) for Eqs. (7), (8), (13) and (14) are

$$v_c^1(\mathbf{x}_c) = v_* \text{ on } \partial\Omega_{\square}^c, \quad (15)$$

$$v_c^2(\mathbf{x}_c) = 0 \text{ on } \partial\Omega_{\square}^c, \quad (16)$$

$$\mathbf{v}_c(\mathbf{x}_c) = \mathbf{0} \text{ on } \partial\Omega_{\square}^c, \quad (17)$$

$$v_c^\alpha(\mathbf{x}_c) = \frac{d[R(\theta)]_{\alpha\beta}}{dt} [\psi^{t\beta}(\mathbf{x}_c) - f^\beta] \text{ on } \partial\Omega_{\square}^c, \quad (18)$$

$$\eta_F \frac{\partial v_c^\alpha}{\partial x_c^1} = 0 \text{ on } \partial\Omega_{\square}^c, \quad (19)$$

$$\sigma_c(\mathbf{x}_c) = 0 \text{ on } \partial\Omega_{\square}^c. \quad (20)$$

Equations (15) and (16) ensure that \mathbf{F} is injected on the boundary $\partial\Omega_{\square}^c$ in a direction parallel to

the x_c^1 axis, and Eq. (17) is a no-slip BC [5] along the channel walls $\partial\Omega_{\square}^c$, see Fig. 1. Equation (18) ensures that, at the boundary $\partial\Omega_{\square}^c$, the \mathbf{F} velocity matches the rotational velocity of \mathbf{R} . Given that \mathbf{R} can only rotate about its left focal point \mathbf{f} , the \mathbf{R} rotational velocity of a point $\mathbf{x}_c \in \partial\Omega_{\square}^c$ is given by

$$\frac{d[R(\theta)]_{\alpha\beta}}{dt}[\psi^{t\beta}(\mathbf{x}_c) - c_\beta], \quad (21)$$

where \mathbf{R} is the rotation matrix corresponding to a counterclockwise rotation:

$$\mathbf{R}(\theta) \equiv \begin{pmatrix} \cos \theta & -\sin \theta \\ \sin \theta & \cos \theta \end{pmatrix}. \quad (22)$$

Finally, Eqs. (19) and (20) ensure, respectively, that on $\partial\Omega_{\square}^c$ there is zero traction and tension; this corresponds to the hypothesis that there is free flow at $\partial\Omega_{\square}^c$ [5, 8].

2. Equations of motion in the reference-configuration coordinates

For each field $\mathbf{v}_c(\mathbf{x}_c), \sigma_c(\mathbf{x}_c)$ which depends on the coordinate \mathbf{x}_c in the c configuration, we introduce its counterpart in the r configuration:

$$\mathbf{v}_c(\mathbf{x}_r, t) \equiv \mathbf{v}_r(\varphi^t(\mathbf{x}_r), t), \quad (23)$$

$$\sigma_c(\mathbf{x}_r, t) \equiv \sigma_r(\varphi^t(\mathbf{x}_r), t). \quad (24)$$

We will now rewrite the equations of motion and the BCs in terms of \mathbf{v}_c, σ_c , and the r coordinate \mathbf{x}_r . The equations of motion (13) and (14) yield

$$\rho_F \left\{ \frac{\partial v_r^\alpha(\mathbf{x}_r, t)}{\partial t} + \left[v_r^\gamma(\mathbf{x}_r, t) - \frac{d\varphi^t(\mathbf{x}_r)}{dt} \right] G_{\beta\gamma}(\mathbf{u}_D^t(\mathbf{x}_r)) \frac{\partial v_r^\alpha(\mathbf{x}_r, t)}{\partial x_r^\beta} \right\} = G_{\beta\alpha}(\mathbf{u}_D^t(\mathbf{x}_r)) \frac{\partial \sigma_r(\mathbf{x}_r, t)}{\partial x_r^\beta} + \eta_F G_{\delta\beta}(\mathbf{u}_D^t(\mathbf{x}_r)) \frac{\partial}{\partial x_r^\delta} \left[G_{\gamma\beta}(\mathbf{u}_D^t(\mathbf{x}_r)) \frac{\partial v_r(\mathbf{x}_r, t)}{\partial x_r^\gamma} \right], \quad (25)$$

$$G_{\beta\alpha}(\mathbf{u}_D^t(\mathbf{x}_r)) \frac{\partial v_r^\alpha(\mathbf{x}_r, t)}{\partial x_r^\beta} = 0, \quad (26)$$

which hold in Ω^r .

The BCs (15) to (20) are rewritten as

$$v_r^1(\mathbf{x}_r) = v_* \text{ on } \partial\Omega_{\square}^r, \quad (27)$$

$$v_r^2(\mathbf{x}_r) = 0 \text{ on } \partial\Omega_{\square}^r, \quad (28)$$

$$\mathbf{v}_r(\mathbf{x}_r) = \mathbf{0} \text{ on } \partial\Omega_{\square}^r, \quad (29)$$

$$v_r^\alpha(\mathbf{x}_r) = \frac{d[R(\theta)]_{\alpha\beta}}{dt}[x_r^\beta - f^\beta] \text{ on } \partial\Omega_{\square}^r, \quad (30)$$

$$\eta_F G_{\beta 1}(\mathbf{u}_D^t(\mathbf{x}_r)) \frac{\partial v_r^\alpha}{\partial x_r^\beta} = 0 \text{ on } \partial\Omega_{\square}^r, \quad (31)$$

$$\sigma_r(\mathbf{x}_r) = 0 \text{ on } \partial\Omega_{\square}^r. \quad (32)$$

C. Motion of bulk fluid domain

The equations of motion (10) and (25) to (32) involve the displacement field \mathbf{u}_D , which describes

how the region—or domain—which contains \mathbf{F} , is deformed in time, cf. Fig. 1. We will denote this region as the \mathbf{D} . We observe that this field has, so far, been left arbitrary, and we have the freedom to choose it.

Here, \mathbf{u}_D will be determined with an analogy with the theory of elasticity [2]. We imagine that, as \mathbf{R} rotates about its focal point, each point $\mathbf{x}_r \in \Omega^r$ moves into a point $\mathbf{x}_c \in \Omega^c$, and that the domain Ω^r is deformed, e.g., locally stretched and compressed, into Ω^c , like an elastic medium.

We will thus determine \mathbf{u}_D as the solution of a boundary-value problem (BVP) given by the following elastic model [2, 9]

$$\frac{\partial S_{D\alpha\beta}(\mathbf{u}_D)}{\partial x_r^\beta} = 0 \text{ in } \Omega^r, \quad (33)$$

where the elastic stress tensor S_D is given by

$$S_{D\alpha\beta} \equiv F_{\alpha\gamma} T_{\gamma\beta}, \quad (34)$$

(39) and (40), we obtain, respectively,

$$\frac{\partial}{\partial x_r^\beta} \frac{dS_{D\alpha\beta}(\mathbf{u}_D)}{dt} = 0 \text{ in } \Omega^r, \quad (41)$$

and

$$\begin{aligned} \dot{\mathbf{u}}_D &= \mathbf{0} \text{ on } \partial\Omega_\square^r, \\ \dot{\mathbf{u}}_D &= \omega \frac{d\mathbf{R}}{d\theta} \cdot (\mathbf{x}_r - \mathbf{f}) \text{ on } \partial\Omega_\circlearrowleft^r, \end{aligned} \quad (42) \quad (43)$$

$$T_{\alpha\beta} \equiv K(\mathbf{u}_D) E_{\gamma\gamma} \delta_{\alpha\beta} + 2\mu(\mathbf{u}_D) \left[E_{\alpha\beta} - \frac{1}{2} \delta_{\alpha\beta} E_{\gamma\gamma} \right], \quad (35)$$

$$E_{\alpha\beta} \equiv \frac{1}{2} (F_{\gamma\alpha} F_{\gamma\beta} - \delta_{\alpha\beta}), \quad (36)$$

$$K(\mathbf{u}) \equiv \frac{1}{[\det(F(\mathbf{u}))]^\zeta}, \quad (37)$$

$$\mu(\mathbf{u}) \equiv \frac{1}{[\det(F(\mathbf{u}))]^\zeta}. \quad (38)$$

In Eqs. (37) and (38), we included an additional dependence of bulk modulus K and the modulus of compression μ on the deformation-gradient tensor (2). In the absence of this dependence, the elastic model above would be unstable under local compression. In fact, the model's Lagrangian would not penalize configurations with small $\det F$. The inclusion of the dependence (37) and (38) on $\det F$ allows for penalizing these configurations—the larger the exponent $\zeta > 0$, the stronger the penalty. As a result, this dependence makes the model stable under mesh compression, such as the one shown below \mathbf{R} in Fig. 1B.

The BCs for the partial differential equation (PDE) (33) are

$$\mathbf{u}_D = \mathbf{0} \text{ on } \partial\Omega_\square^r, \quad (39)$$

$$\mathbf{u}_D = \mathbf{f} - \mathbf{x}_r + \mathbf{R}(\theta) \cdot (\mathbf{x}_r - \mathbf{f}) \text{ on } \partial\Omega_\circlearrowleft^r. \quad (40)$$

Equation (39) enforces the fact that the mesh is not deformed at the boundary $\partial\Omega_\square^r$. Finally, Eq. (40) ensures that the mesh deformation at $\partial\Omega_\circlearrowleft^r$ matches the deformation induced by the rotation of \mathbf{R} .

Equations (33), (39) and (40) constitute the BVP which determines \mathbf{u}_D . Along the lines of BVPs in the theory of elasticity, such BVP is already, naturally formulated in the \mathbf{r} configuration [3].

From the BVP above, we obtain a BVP for $\dot{\mathbf{u}}_D$, which will be needed in the following to describe the \mathbf{D} motion. By deriving both sides of Eqs. (33),

where in Eqs. (42) and (43) we used the fact that \mathbf{x}_r is independent of time, and in Eq. (43) we substituted Eq. (8). The left-hand side (LHS) of Eq. (41) depends on the second partial derivatives of \mathbf{u}_D and $\dot{\mathbf{u}}_D$ —see Eqs. (34) to (38). As a result, given θ , ω , and \mathbf{u}_D from Eqs. (33), (39) and (40), the BVP (41) to (43) yields $\dot{\mathbf{u}}_D$.

Overall Eqs. (8), (10), (25) to (33) and (39) to (43) constitute a BVP for $\theta, \omega, \mathbf{v}_r, \sigma_r, \mathbf{u}_D$ and $\dot{\mathbf{u}}_D$ which, combined with the temporal BCs

$$\theta(t=0) = \theta_0 \quad (44)$$

$$\omega(t=0) = \omega_0 \quad (45)$$

$$\mathbf{v}_r(\mathbf{x}_r, t=0) = \mathbf{v}_{r0}(\mathbf{x}_r), \quad (46)$$

$$\sigma_r(\mathbf{x}_r, t=0) = \sigma_{r0}(\mathbf{x}_r), \quad (47)$$

determine the dynamics of the system.

D. Temporal discretization

To numerically solve for the dynamics in a time span $0 \leq t \leq T$, we discretize time by setting $\Delta t \equiv T/N$, $t_n \equiv n \Delta t$, with $n = 0, 1, \dots, N$.

We combine the Crank Nicolson (CN) discretization method for NS equations [8, 10] with the ALE formulation, by discretizing the dynamical equations for \mathbf{R} , \mathbf{F} and \mathbf{D} —see below.

1. Rigid body

Proceeding along the CN scheme [10], we define fields at staggered, integer and semi-integer time steps scheme [8]. We set

$$\sigma_r^n(\mathbf{x}_r) \equiv \sigma_c(\mathbf{x}_r, t_n) \quad (48)$$

$$\sigma_r^{n-1/2}(\mathbf{x}_r) \equiv \sigma_c \left(\mathbf{x}_r, \frac{t_n + t_{n-1}}{2} \right), \quad (49)$$

and similarly for other quantities.

We discretize Eqs. (8) and (10) and, neglecting $\mathcal{O}(\Delta t)$, we obtain

$$\frac{\theta^n - \theta^{n-1}}{\Delta t} = \omega^n, \quad (50)$$

$$\frac{\omega^n - \omega^{n-1}}{\Delta t} = I \int_{\partial\Omega_r^c} ds \epsilon_{\alpha\beta} [\xi^\alpha(s) + u^{n-1,\alpha}(\xi(s)) - f^\alpha] \varsigma_{\beta\gamma}^{r,n-1}(\xi(s); \mathbf{v}_r^{n-1}, \sigma_r^{n-3/2}) \times \epsilon_{\gamma\lambda} F_{\lambda\mu}(\mathbf{u}_D^{n-1}(\xi(s))) \frac{d\xi^\mu(s)}{ds}, \quad (51)$$

where in Eq. (51) we used Eqs. (1) and (5) and we explicitly indicated the dependence of the stress tensor (11) on \mathbf{v}_c and σ_c .

2. Bulk fluid

To discretize in time the **F** problem, we will apply the **CN** splitting scheme [8, 10] to the **NS** equations

(25) and (26) in the **r** configurations. This splitting scheme is derived from the **incremental pressure correction scheme** [11], in which the solution of the **NS** equations is split into three intermediate steps. In what follows, we will synonymously use the terms ‘pressure’ and ‘surface tension’ for conciseness [12].

The discrete form of the PDEs Eqs. (25) and (26) is

$$\rho_F \left[\frac{v_r^{n,\alpha} - v_r^{n-1,\alpha}}{\Delta t} + \frac{3}{2}(v_r^{n-1,\gamma} - \dot{u}^{n-1,\gamma}) G_{\beta\gamma}(\mathbf{u}_D^{n-1}) \frac{\partial v_r^{n-1,\alpha}}{\partial x_r^\beta} - \frac{1}{2}(v_r^{n-2,\gamma} - \dot{u}^{n-2,\gamma}) \times \right. \quad (52)$$

$$\left. G_{\beta\gamma}(\mathbf{u}_D^{n-2}) \frac{\partial v_r^{n-2,\alpha}}{\partial x_r^\beta} \right] = G_{\beta\alpha}(\mathbf{u}_D^{n-1}) \frac{\partial \sigma_r^{n-1/2}}{\partial x_r^\beta} + \eta_F G_{\delta\beta}(\mathbf{u}_D^{n-1}) \frac{\partial}{\partial x_r^\delta} \left[G_{\gamma\beta}(\mathbf{u}_D^{n-1}) \frac{\partial}{\partial x_r^\gamma} \left(\frac{v_r^{n,\alpha} + v_r^{n-1,\alpha}}{2} \right) \right], \\ G_{\beta\alpha}(\mathbf{u}_D^{n-1}) \frac{\partial v_r^{n,\alpha}}{\partial x_r^\beta} = 0, \quad (53)$$

where we omitted the dependence on \mathbf{x}_r for clarity. Also, in the **LHS** of Eq. (52) we rewrote the convective term according to the Adams-Bashforth discretization scheme [8, 13], and we used Eqs. (1)

and (5) to rewrite the time derivative of φ in terms of $\dot{\mathbf{u}}_D$.

The discrete form of the **BCs** (27) to (32) reads

$$v_r^{n,1} = v_* \text{ on } \partial\Omega_{\square}^r, \quad (54)$$

$$v_r^{n,2} = 0 \text{ on } \partial\Omega_{\square}^r, \quad (55)$$

$$\mathbf{v}_r^n = \mathbf{0} \text{ on } \partial\Omega_{\square}^r, \quad (56)$$

$$\mathbf{v}_r = \omega^n \left. \frac{d\mathbf{R}}{d\theta} \right|_{\theta=\theta_n} \cdot (\mathbf{x}_r - \mathbf{f}) \text{ on } \partial\Omega_{\square}^r, \quad (57)$$

$$\eta_F G_{\beta 1}(\mathbf{u}_D^{n-1}) \frac{\partial}{\partial x_r^\beta} \left(\frac{v_r^{n,\alpha} + v_r^{n-1,\alpha}}{2} \right) = 0 \text{ on } \partial\Omega_{\square}^r, \quad (58)$$

$$\sigma_r^{n-1/2} = 0 \text{ on } \partial\Omega_{\square}^r. \quad (59)$$

We will now split the **BVP** into three steps [8, 14]:

the velocity $\bar{\mathbf{v}}$, which approximates the true velocity \mathbf{v}_r , and which satisfies the **BVP**

1. Approximated velocity. We introduce

$$\rho_F \left\{ \frac{\bar{v}^\alpha - v_r^{n-1,\alpha}}{\Delta t} + \left[\frac{3}{2}(v_r^{n-1,\gamma} - \dot{u}^{n-1,\gamma}) G_{\beta\gamma}(\mathbf{u}_D^{n-1}) - \frac{1}{2}(v_r^{n-2,\gamma} - \dot{u}^{n-2,\gamma}) G_{\beta\gamma}(\mathbf{u}_D^{n-2}) \right] \frac{\partial V^\alpha}{\partial x_r^\beta} \right\} = (60)$$

$$G_{\beta\alpha}(\mathbf{u}_D^{n-1}) \frac{\partial \sigma_r^*}{\partial x_r^\beta} + \eta_F G_{\delta\beta}(\mathbf{u}_D^{n-1}) \frac{\partial}{\partial x_r^\delta} \left(G_{\gamma\beta}(\mathbf{u}_D^{n-1}) \frac{\partial V^\alpha}{\partial x_r^\gamma} \right),$$

$$\bar{v}^1 = v_* \text{ on } \partial\Omega_{\square}^r, \quad (61)$$

$$\bar{v}^2 = 0 \text{ on } \partial\Omega_{\square}^r, \quad (62)$$

$$\bar{\mathbf{v}} = \mathbf{0} \text{ on } \partial\Omega_{\square}^r, \quad (63)$$

$$\bar{\mathbf{v}} = \omega^n \left. \frac{d\mathbf{R}}{d\theta} \right|_{\theta=\theta_n} \cdot (\mathbf{x}_r - \mathbf{f}) \text{ on } \partial\Omega_{\square}^r, \quad (64)$$

$$\eta_F G_{\beta 1}(\mathbf{u}_D^{n-1}) \frac{\partial V^\alpha}{\partial x_r^\beta} = 0 \text{ on } \partial\Omega_{\square}^r. \quad (65)$$

where

$$\mathbf{V} \equiv \frac{\bar{\mathbf{v}} + \mathbf{v}_r^{n-1}}{2}, \quad (66)$$

$$\sigma_r^* \equiv \sigma_r^{n-3/2}. \quad (67)$$

2. Pressure correction.

Subtracting Eqs. (52) and (60) and neglecting $\mathcal{O}(\Delta t)$, we obtain

$$\rho_F \frac{\bar{v}^\alpha - v_r^{n,\alpha}}{\Delta t} = G_{\beta\alpha}(\mathbf{u}_D^{n-1}) \frac{\partial \phi}{\partial x_r^\beta} \text{ in } \Omega^r, \quad (68)$$

where

$$\phi \equiv \sigma_c^* - \sigma_c^{n-1/2} \quad (69)$$

is the surface-tension increment. By applying $G_{\gamma\alpha}(\mathbf{u}_D^{n-1}) \partial/\partial x_r^\gamma$ to both sides of Eq. (68) and using Eq. (53), we obtain a second-order PDE for ϕ :

$$\frac{\rho_F}{\Delta t} G_{\gamma\alpha}(\mathbf{u}_D^{n-1}) \frac{\partial \bar{v}^\alpha}{\partial x_r^\gamma} = (70)$$

$$G_{\gamma\alpha}(\mathbf{u}_D^{n-1}) \frac{\partial}{\partial x_r^\gamma} \left(G_{\beta\alpha}(\mathbf{u}_D^{n-1}) \frac{\partial \phi}{\partial x_r^\beta} \right).$$

We will now work out the BCs for Eq. (70). Equations (59), (67) and (69) imply the BC

$$\phi = 0 \text{ on } \partial\Omega_{\square}^r. \quad (71)$$

Multiplying Eq. (68) by $G_{\gamma\alpha}(\mathbf{u}_D^{n-1})\hat{\mathbf{n}}^r\gamma$, where $\hat{\mathbf{n}}^r$ is the unit boundary normal in the r configuration, we obtain

$$\frac{\rho_F}{\Delta t} G_{\gamma\alpha}(\mathbf{u}_D^{n-1})\hat{\mathbf{n}}^r\gamma(\bar{v}^\alpha - v_r^{n,\alpha}) = \quad (72)$$

$$\hat{\mathbf{n}}^r\gamma G_{\gamma\alpha}(\mathbf{u}_D^{n-1})G_{\beta\alpha}(\mathbf{u}_D^{n-1})\frac{\partial\phi}{\partial x_r^\beta}.$$

Combining Eq. (72) with Eqs. (54) to (57) and (61) to (64), we obtain the second BC

$$\hat{\mathbf{n}}^r\gamma G_{\gamma\alpha}(\mathbf{u}_D^{n-1})G_{\beta\alpha}(\mathbf{u}_D^{n-1})\frac{\partial\phi}{\partial x_r^\beta} = \quad (73)$$

$$0 \text{ on } \partial\Omega_D^r \cup \partial\Omega_\square^r \cup \partial\Omega_\bullet^r.$$

The BVP (70), (71) and (73) determines ϕ and, through the definition (69), the surface tension $\sigma_c^{n-1/2}$.

- 3. Velocity correction.** The velocity \mathbf{v}_r^n is determined from the approximate velocity $\bar{\mathbf{v}}$ from Eq. (68).

3. Bulk fluid domain

The discrete version of the BVP for \mathbf{u}_D , Eqs. (33), (39) and (40), reads

$$\frac{\partial S_{D\alpha\beta}(\mathbf{u}_D^n)}{\partial x_r^\beta} = 0 \text{ in } \Omega^r, \quad (74)$$

$$\mathbf{u}_D^n = \mathbf{0} \text{ on } \partial\Omega_\square^r, \quad (75)$$

$$\mathbf{u}_D^n = \mathbf{f} - \mathbf{x}_r + \mathbf{R}(\theta^n) \cdot (\mathbf{x}_r - \mathbf{f}) \text{ on } \partial\Omega_\bullet^r, \quad (76)$$

and that of the BVP for $\dot{\mathbf{u}}_D$, Eqs. (41) to (43), is

$$\frac{\partial}{\partial x_r^\beta} \frac{dS_{D\alpha\beta}(\dot{\mathbf{u}}_D^n)}{dt} = 0 \text{ in } \Omega^r, \quad (77)$$

$$\dot{\mathbf{u}}_D^n = \mathbf{0} \text{ on } \partial\Omega_\square^r, \quad (78)$$

$$\dot{\mathbf{u}}_D^n = \omega \frac{d\mathbf{R}}{d\theta} \cdot (\mathbf{x}_r - \mathbf{f}) \text{ on } \partial\Omega_\bullet^r, \quad (79)$$

We can now iterate in time for the ensemble of fields as follows. At each step n , given θ^{n-1} , ω^{n-1} , \mathbf{v}_r^{n-1} , $\sigma_r^{n-3/2}$, \mathbf{u}_D^{n-1} and $\dot{\mathbf{u}}_D^{n-1}$ from the preceding step, we

- 1. Update R.** Solve the algebraic equations Eqs. (50) and (51) for θ^n and ω^n .

- 2. Update D.** Solve the BVPs (74) to (79) for \mathbf{u}_D^n and $\dot{\mathbf{u}}_D^n$.

- 3. Update F.** Solve the BVPs (60) to (65) and (71) to (73) for $\bar{\mathbf{v}}$ and $\sigma_r^{n-1/2}$, and obtain \mathbf{v}_r^n from Eq. (68).

The fields \mathbf{v}_r^{n-1} , $\sigma_r^{n-3/2}$ in the c configuration are then obtained from the respective fields in the r configuration through Eqs. (23) and (24).

An example of such dynamics is shown in Fig. 2. The channel has dimensions $L = 2.2$ m, $h = 0.41$ m, cf. Fig. 1, $\rho_F = 1$ Kg/m², $\eta_F = 10^{-3}$ Pa m sec, and the inflow velocity profile is a Poiseuille flow $v_*(\mathbf{x}_c) = 6v_0x_c^2(x_c^2 - h)/h^2$, with $v_0 = 1$ m/sec. These parameters have been taken from the FEAT2D DFG 2D-3 benchmark for a flow around a cylinder [15]. The D mesh stiffness exponent has been chosen to be $\zeta = 3$ [2]. Finally, R is an ellipse with semi-axes $a = 0.1$ m, $b = 0.075$ m, center located at $\mathbf{x}_r = (0.25$ m, 0.2 m), and moment of inertia $I = 10^{-1}$ Kg m². These parameters correspond approximately to a light gas interacting with a solid body made of light wood.

As shown in Fig. 3, the dynamics of Fig. 2 involves two physical time scales: A short one, τ_S , related to fast angular oscillations of B , and a long one, τ_L , given by the damping of such oscillations.

First, the scale τ_S can be estimated by considering the dynamical equation (7) for B , and approximating its LHS as I/τ_S^2 and its RHS as $(\eta_F v_0/a)2\pi a$. Here, $\eta_F v_0/a$ is the viscous component of the force per unit length exerted by F on B , cf. Eq. (9), $2\pi a$ estimates the total length of the boundary of B , and a approximates the lever arm of the force above. Putting everything together, we obtain

$$\tau_S \sim \sqrt{\frac{I}{2\pi a \eta_F v_0}}. \quad (80)$$

For the parameters of Fig. 2, Eq. (80) yields $\tau_S \sim 13$ sec, which is in agreement with the period of the oscillations in Fig. 3.

Second, τ_L can be estimated by building a combination of the material parameters ρ_F , η_F and I of the model. The only parameter combination that can yield a quantity with the dimensions of a time is

$$\tau_L \sim \frac{\sqrt{\rho_F I}}{\eta_F}. \quad (81)$$

For the parameters of Fig. 2, Eq. (81) yields $\tau_L \sim 316$ sec, which is roughly the timescale at which

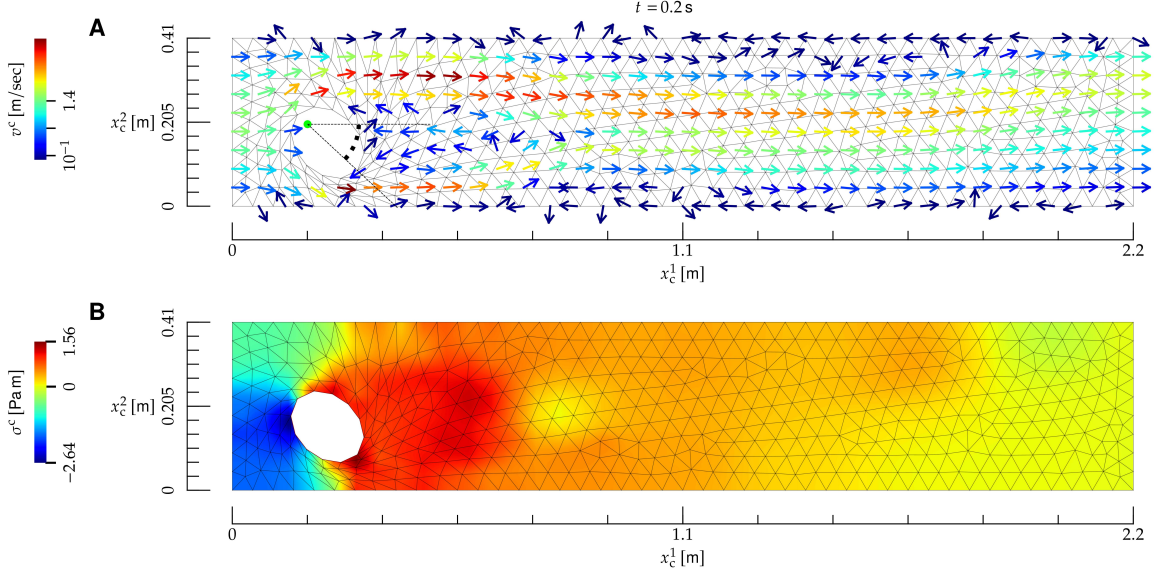


FIG. 2: Interaction between a **bulk fluid** and a rigid **body**, whose material properties roughly correspond to a light gas and a body made of light wood, respectively. **A)** Temporal snapshot of the mesh (black lines) and velocity field (arrows) at the **current** time t , shown on top. The direction of the velocity field is indicated by the arrows, and its norm by their color; the direction of arrows with velocity close to zero is not defined. The **body** (ellipse) is allowed to pivot about its left focal point (red dot), and the related angle with respect to the x_c^1 direction is denoted by a red arc. **B)** Color map of the surface tension at the **current** instant of time t .

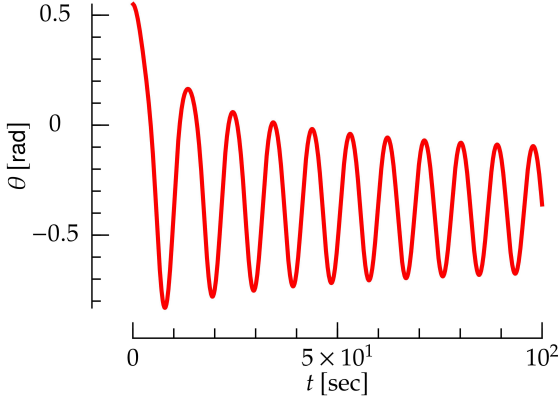


FIG. 3: Angle of the **body** as a function of time for the interaction between a **bulk fluid** and a rigid **body** shown in Fig. 2.

the width of the oscillations in Fig. 3 is damped out.

II. FLUID AND ELASTIC BODY

In this Section, we will build on the analysis of Section I and put F into interaction with a more complex physical object: an **elastic body** (E). Only the main results will be presented here; their derivation follows the lines of Section I.

The **r** and **c** configurations are shown in Fig. 4. Here, the **E** boundary $\partial\Omega_E$ may deform, but the inner **E** boundary $\partial\Omega_{\bullet}$ is pinned to the x^1 , x^2 plane.

The equations of motion are the following.

First, the dynamics of F is governed by the NS and mass-conservation equations (13) and (14), respectively. Their BCs are Eqs. (15) to (17), (19) and (20), which stay unchanged. On the other hand, BC (18), which ensures that the F velocity matches the B velocity at the interface between F and B, now reads

$$\mathbf{v}_c(\mathbf{x}_c) = \frac{d\mathbf{u}_E(\mathbf{x}_r)}{dt} \Big|_{\mathbf{x}_r=\psi^t(\mathbf{x}_c)} \quad \text{on } \partial\Omega_E^c \quad (82)$$

Second, the motion of E is governed by Newton's

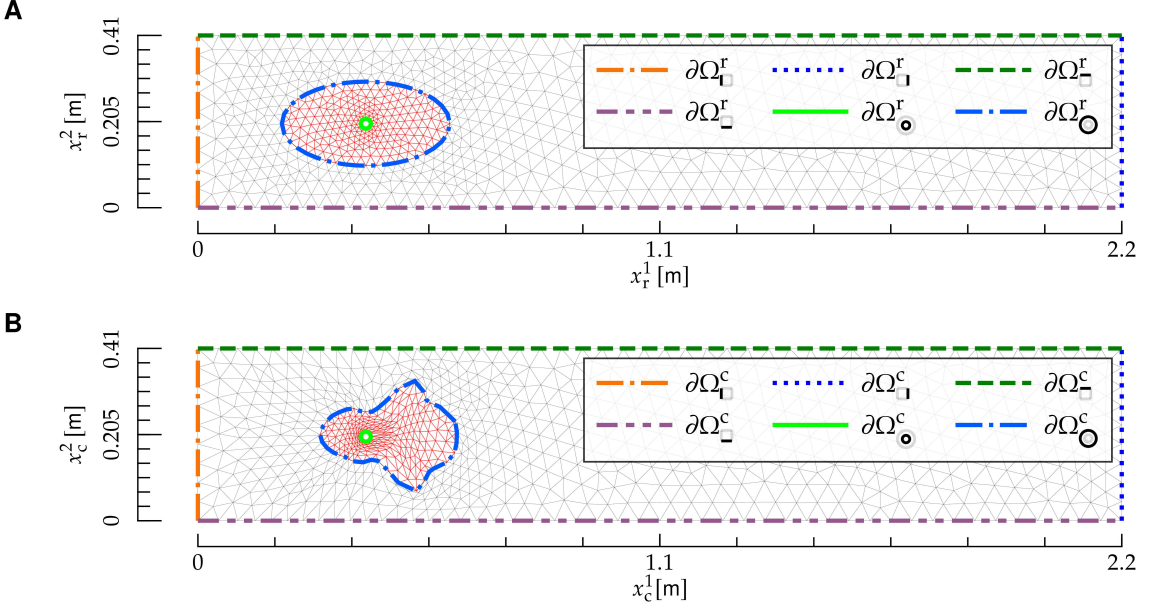


FIG. 4: Reference and current configuration for the interaction between a bulk fluid and an elastic body. The figures follows the same notation as Fig. 1.

equations of motion for an elastic body [3]

$$\rho_E \frac{d^2 u_E^\alpha(x_r)}{dt^2} = \frac{\partial S_{E\alpha\beta}(u_E)}{\partial x_r^\beta}, \quad (83)$$

where u_E and ρ_E are, respectively, the deformation field and density of E; the latter is assumed to be independent of space. The E stress tensor is derived from a compressible neo-Hookean model [16], and it reads

$$S_{E\alpha\beta} \equiv \frac{\mu}{\det(F)} \left(-\frac{1}{2} C_{\gamma\gamma} G_{\alpha\beta} + F_{\beta\alpha} \right) + K[(\det(F))^2 - 1] G_{\alpha\beta}, \quad (84)$$

where

$$C_{\alpha\beta} \equiv \delta_{\alpha\beta} + 2E_{\alpha\beta}. \quad (85)$$

We have chosen this model because it is stable under compression, i.e., its potential energy diverges as $\det(F) \rightarrow 0$ [16]. As opposed to linear models [3] and to the elastic model of Section I C, this model proves to yield a stable dynamics for E as it is compressed by F, see below and Fig. 5. The BCs

for Eq. (83) are

$$u_E(x_r) = 0 \text{ on } \partial\Omega_r^r, \quad (86)$$

$$\epsilon_{\beta\gamma} S_{E\alpha\beta}(u_E^t)|_{x_r=\xi(s)} \frac{d\xi^\gamma}{ds} = \zeta^c_{\alpha\beta}(\varphi^t(\xi(s))) \epsilon_{\beta\gamma} \frac{d\varphi^{t,\gamma}(\xi(s))}{ds} \text{ on } \partial\Omega_O^r. \quad (87)$$

Finally, the equations of motion for D are (33) and (41), with BCs (39) and (42) and

$$u_D^t(x_r) = u_E^t(x_r) \text{ on } \partial\Omega_O^r, \quad (88)$$

$$\dot{u}_D^t(x_r) = \dot{u}_E^t(x_r) \text{ on } \partial\Omega_O^r. \quad (89)$$

Equation (88) and Eq. (89) ensure that the displacement and velocity of E and D are conformal at the E-D interface, and they replace Eqs. (40) and (43), respectively.

The system dynamics is obtained as follows: given v_r^{n-1} , $\sigma_r^{n-3/2}$, u_E^{n-1} , \dot{u}_E^{n-1} , u_D^{n-1} and \dot{u}_D^{n-1} from the preceding step, we

- **Update E.** Solve for u_E^n and \dot{u}_E^n the discrete version of Eq. (83)

$$\rho_E \frac{\dot{u}_E^{n,\alpha} - \dot{u}_E^{n-1,\alpha}}{\Delta t} = \frac{\partial S_{E\alpha\beta}(u_E^n)}{\partial x_r^\beta}, \quad (90)$$

$$\frac{u_E^n - u_E^{n-1}}{\Delta t} = \dot{u}_E, \quad (91)$$

with BCs obtained from Eqs. (86) and (87):

$$\mathbf{u}_E^n = 0 \text{ on } \partial\Omega_{\bullet}^r, \quad (92)$$

$$\epsilon_{\beta\gamma} S_{E\alpha\beta}(\mathbf{u}_E^n) \Big|_{x_r=\xi(s)} \frac{d\xi^\gamma}{ds} = \varsigma^r_{\alpha\beta}(\xi(s); \mathbf{v}_r^{n-1}, \sigma_r^{n-3/2}, \mathbf{u}^n) \epsilon_{\beta\gamma} F_{\gamma\delta}(\mathbf{u}_E^{n-1}) \Big|_{x_r=\xi(s)} \frac{d\xi^\delta}{ds} \text{ on } \partial\Omega_{\bullet}^r. \quad (93)$$

In Eq. (93), we have used Eqs. (2) and (5) to rewrite the derivative of $\phi(\xi(s))$.

- **Update D.** Solve for \mathbf{u}_D^n and $\dot{\mathbf{u}}_D^n$ the BVPs given by Eqs. (74) and (77) with BCs (75), (78) and

$$\mathbf{u}_D^n = \mathbf{u}_E^n \text{ on } \partial\Omega_{\bullet}^r, \quad (94)$$

$$\dot{\mathbf{u}}_D^n = \dot{\mathbf{u}}_E^n \text{ on } \partial\Omega_{\bullet}^r. \quad (95)$$

- **Update F.** Solve the BVPs given by (60) and (70) and BCs (61) to (63), (65), (71) and (73) and

$$\mathbf{v}_r = \dot{\mathbf{u}}_E \text{ on } \partial\Omega_{\bullet}^r, \quad (96)$$

which replaces Eq. (65) for a rigid body, and solve Eq. (68).

An example of the coupled dynamics of \mathbf{F} and \mathbf{E} is shown in Fig. 5. Here, $\partial\Omega_{\bullet}^r$ is an ellipse

with semi-axes $a = 0.2 \text{ m}$, $b = 0.1 \text{ m}$ and center located at $x_r = (0.4 \text{ m}, 0.2 \text{ m})$, and $\partial\Omega_{\bullet}^r$ has radius $r = 0.0125 \text{ m}$ and center located at x_r . The \mathbf{E} density and elastic moduli are, respectively, $\rho_E = 10^3 \text{ Kg/m}^2$ and $K = \mu = 10 \text{ Kg/sec}^2$. The other parameters are the same as in Fig. 2.

ACKNOWLEDGMENTS

We would like to thank S. Al-Izzi and S. Astruc for useful discussions, and the finite element computational software (FEniCS) online community for its precious support.

This work was granted access to the high-performance computing resources of MesoPSL financed by the Region Île de France, and to the Abacus cluster at Institut Curie.

- [1] I. Derényi, F. Jülicher, and J. Prost. Formation and Interaction of Membrane Tubes. *Phys. Rev. Lett.*, 88(23):238101, May 2002.
- [2] D. Kamensky. Lecture notes for MAE 207: Finite element analysis for coupled problems, 2022.
- [3] L. D. Landau and E. M. Lifshitz. *Theory of Elasticity*. Elsevier, 1986.
- [4] W. S. Slaughter. *The Linearized Theory of Elasticity*. Birkhäuser Boston, Boston, MA, 2002.
- [5] L. D. Landau and E. M. Lifschitz. *Fluid Mechanics*. Pergamon, 1987.
- [6] H. Goldstein, C. P. Poole, and J. L. Safko. *Classical Mechanics*. Pearson, 2004.
- [7] S. Marchiafava. *Appunti Di Geometria Differenziale*, volume I, II, III. Edizioni Nuova Cultura, 2005.
- [8] A. Logg, K.-A. Mardal, and G. Wells, editors. *Automated Solution of Differential Equations by the Finite Element Method: The FEniCS Book*, volume 84 of *Lecture Notes in Computational Science and Engineering*. Springer Berlin Heidelberg, Berlin, Heidelberg, 2012.
- [9] J. E. Marsden and T. J. R. Hughes. *Mathematical Foundations of Elasticity*. Dover, New York, 1994.
- [10] J. Crank and P. Nicolson. A practical method for numerical evaluation of solutions of partial differential equations of the heat-conduction type. *Math. Proc. Camb. Phil. Soc.*, 43(1):50–67, Jan. 1947.
- [11] K. Goda. A multistep technique with implicit difference schemes for calculating two- or three-dimensional cavity flows. *Journal of Computational Physics*, 30(1):76–95, Jan. 1979.
- [12] D. Wörthmüller, G. Ferraro, P. Sens, and M. Castellana. IRENE: A fluId layeR finitElemeNt softwarE, July 2025.
- [13] *Solving Ordinary Differential Equations I*, volume 8 of *Springer Series in Computational Mathematics*. Springer Berlin Heidelberg, Berlin, Heidelberg, 1993.
- [14] A. J. Chorin. Numerical solution of the Navier-

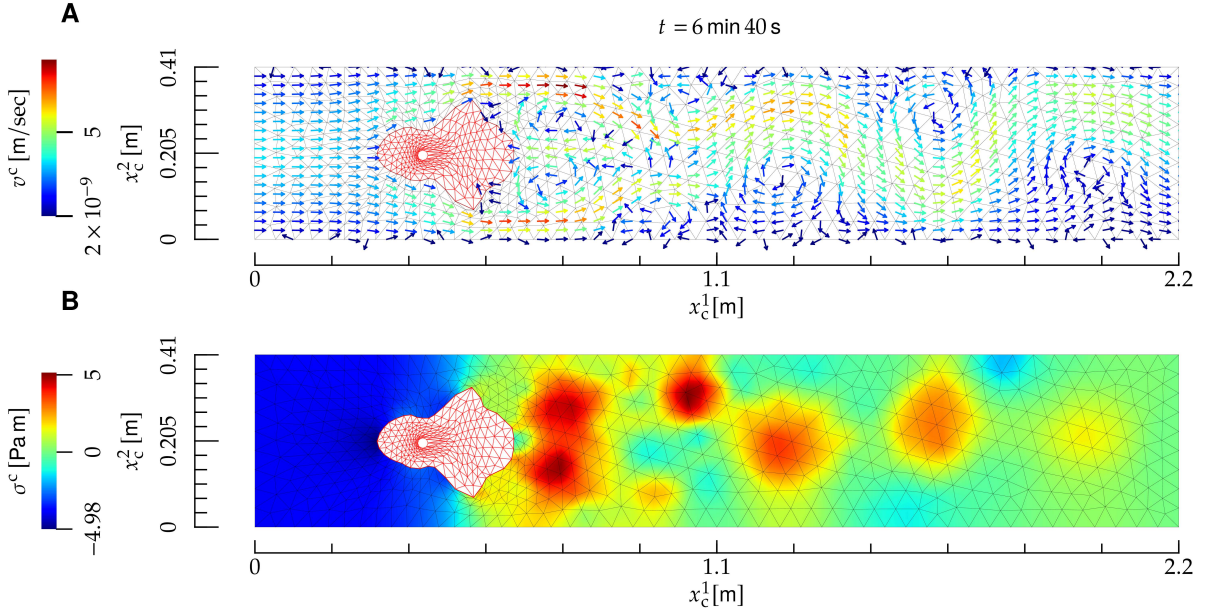


FIG. 5: Interaction between a **bulk fluid** and an **elastic body**. The notation is the same as in Fig. 2, and the **elastic body** is depicted as a red mesh.

- Stokes equations. *Math. Comp.*, 22(104):745–762, 1968.
[15] H. Blum, J. Harig., S. Müller, S. Schreiber, and S. Turek. FEAT2D, Finite Element Analysis Tools

- User Manual, 1995.
[16] Y. Bazilevs, V. M. Calo, T. J. R. Hughes, and Y. Zhang. Isogeometric fluid-structure interaction: Theory, algorithms, and computations. *Comput Mech*, 43(1):3–37, Dec. 2008.

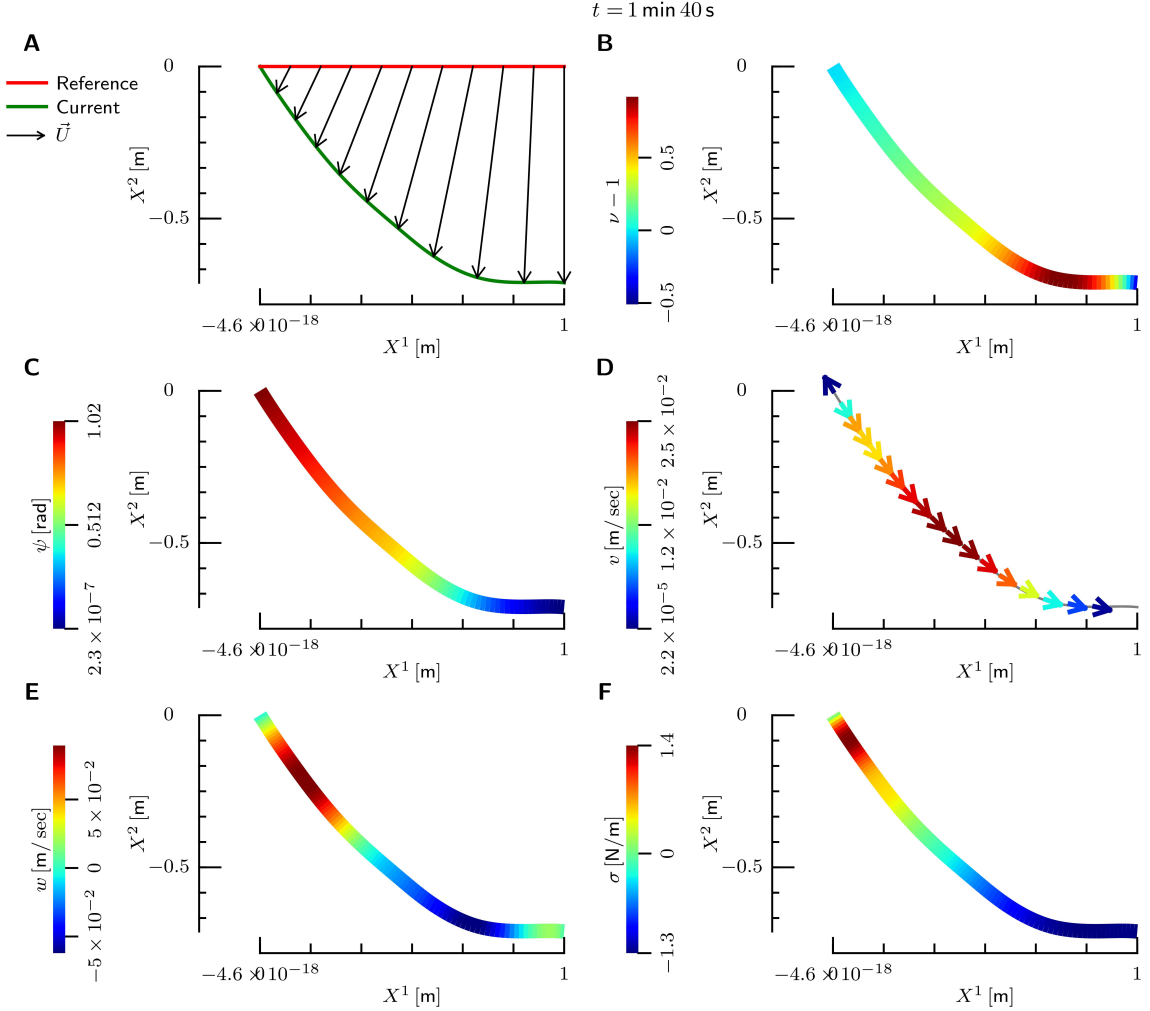


FIG. 6: Helfrich fluid layer described with the generalized arc length gauge. The layer is subjected to a gravitational field directed along the X^2 axis, in the direction of negative X^2 . **A)** Displacement field \vec{U} , which relates the reference and the current configuration, shown in red and green, respectively. **B)** Stretching ν . **C)** Tangent angle ψ . **D)** Tangential velocity. Arrows show the velocity direction, and the color code the velocity norm. **E)** Normal velocity, whose value is shown with the color code. **F)** Surface tension. All panels refer to the same instant of time, shown on top.

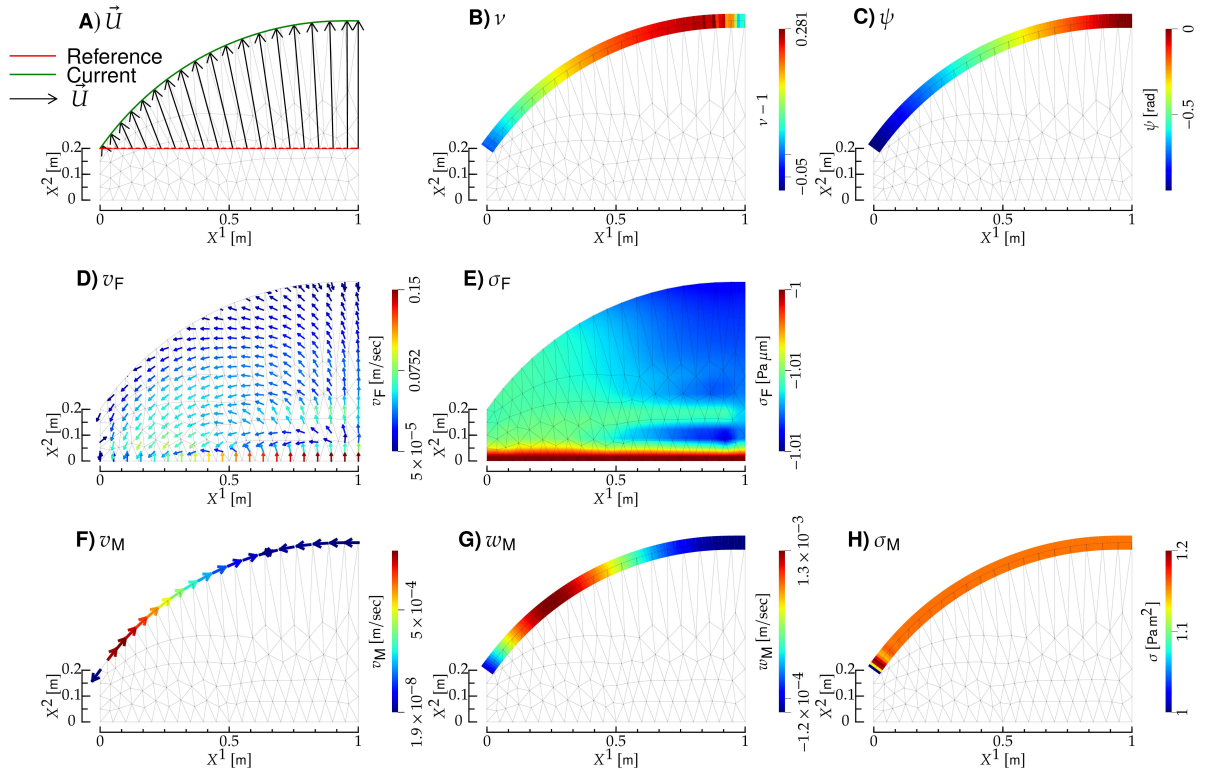


FIG. 7: Interaction between a bulk fluid and a Helfrich membrane. **A)** Membrane reference and current configuration (red and green curve, respectively), and displacement field (black arrows). **B)** Membrane stretch field. **C)** Membrane tangent angle. **D)** and **E)** Bulk-fluid velocity and tension; the notation is the same as in Fig. 2. **F)**, **G)** and **H)**: membrane tangential velocity, normal velocity and tension; the notation is the same as in Fig. 6B, C and D, respectively. All panels refer to the same instant of time, shown on top, and display also the deformed mesh (gray lines).